JOURNAL OF MATERIALS SCIENCE 23 (1988) 2837–2845

Formation of amorphous Ni–Zr alloy powder by mechanical alloying of intermetallic powder mixtures and mixtures of nickel or zirconium with intermetallics

P. Y. LEE, C. C. KOCH
Department of Materials Science and Engineering, North Carolina State University, Raleigh, North Carolina 27695-7907, USA

Mechanical alloying was used to synthesize Ni_xZr_{1-x} alloys from mixtures of intermetallic compound powders, and also from mixtures of intermetallic compound powders and pure elemental powders. The mechanically alloyed powders were amorphous in the range $0.24 \leqslant x \leqslant 0.85$. This range is larger than amorphous alloys produced by the melt-spinning technique and mechanical alloying of elemental crystalline powders. Two-phase mixtures of the amorphous phase and the corresponding crystalline terminal solid solution were formed in the range $0.10 \leqslant x \leqslant 0.22$, and $x = 0.90$. It is found that the morphological development during mechanical alloying of these powders is different from mechanical alloying using only pure ductile crystalline elemental powders. The thermal stability has been investigated. The enthalpy and activation energy of crystallization for Ni–Zr amorphous powders prepared by mechanical alloying are lower than those for melt-spun samples of the same composition. The crystallization temperature of the mechanically alloyed Ni–Zr amorphous powders is higher than that of melt-spun samples in the composition range $Ni_{20}Zr_{80}$ to $Ni_{33}Zr_{67}$ and $Ni_{40}Zr_{60}$ to $Ni_{60}Zr_{40}$. The presence of tiny crystallites as nucleation centres and high oxygen levels in the mechanically alloyed amorphous alloys might be responsible for the differences in crystallization behaviour. A new crystalline metastable phase was observed during crystallization studies of $Ni_{24}Zr_{76}$ amorphous powder.

1. Introduction

Amorphous metallic alloys constitute a new class of metallic materials and have attracted considerable attention in the scientific and technological world over the last two decades [1]. These materials are usually prepared by rapid quenching from the liquid or vapour states. In recent years, the formation of an amorphous phase by solid-state interdiffusion reaction of crystalline materials has been demonstrated as an alternate route in various transition metal alloy systems [2]. Mechanical alloying (MA) is one method of amorphization from the solid crystalline state. This was first established by Koch *et al.* [3], who produced amorphous $Ni_{60}Nb_{40}$ powder by MA of pure crystalline nickel and niobium powders. Subsequently, many amorphous binary transition metal alloys have been formed by MA of the elemental powders [4–6]. The amorphization by MA of pure crystalline powders can be described by a mechanism similar to that which has been used to explain the amorphization of thin films by thermal interdiffusion [7]. It is assumed that a negative heat of mixing provides the thermodynamic driving force which favours interdiffusion. This is consistent with experiment, in that all alloy systems which have been amorphized by MA exhibit negative heats of mixing. However, it has been shown that equilibrium intermetallic compounds can be amorphized by high-energy ball milling [8] (not MA *per se*, because no "alloying" takes place). The amorphization by grinding during such a milling process might be explained by a critical defect mechanism [9]. Davis and Koch [10] recently found that the nominally brittle elements silicon and germanium form a solid solution, i.e. "alloy", during MA. This implies that material transfer can occur even between brittle components by a mechanism not yet fully understood. In this paper, we investigated the formation of amorphous Ni–Zr alloys by a different MA route. Two types of starting powder with different crystalline states were used: (1) mixtures of pure crystalline and intermetallic powders, (2) mixtures of intermetallic powders [11]. The amorphous Ni–Zr powders formed by this method were investigated by X-ray diffraction, scanning electron microscopy (SEM), transmission electron microscopy (TEM) as well as differential scanning calorimetry (DSC).

2. Experimental procedures

Pure nickel (99.9%, metal basis) and zirconium (99%, metal basis) powder were purchased from Alfa

0022–2461/88 $03.00 + .12

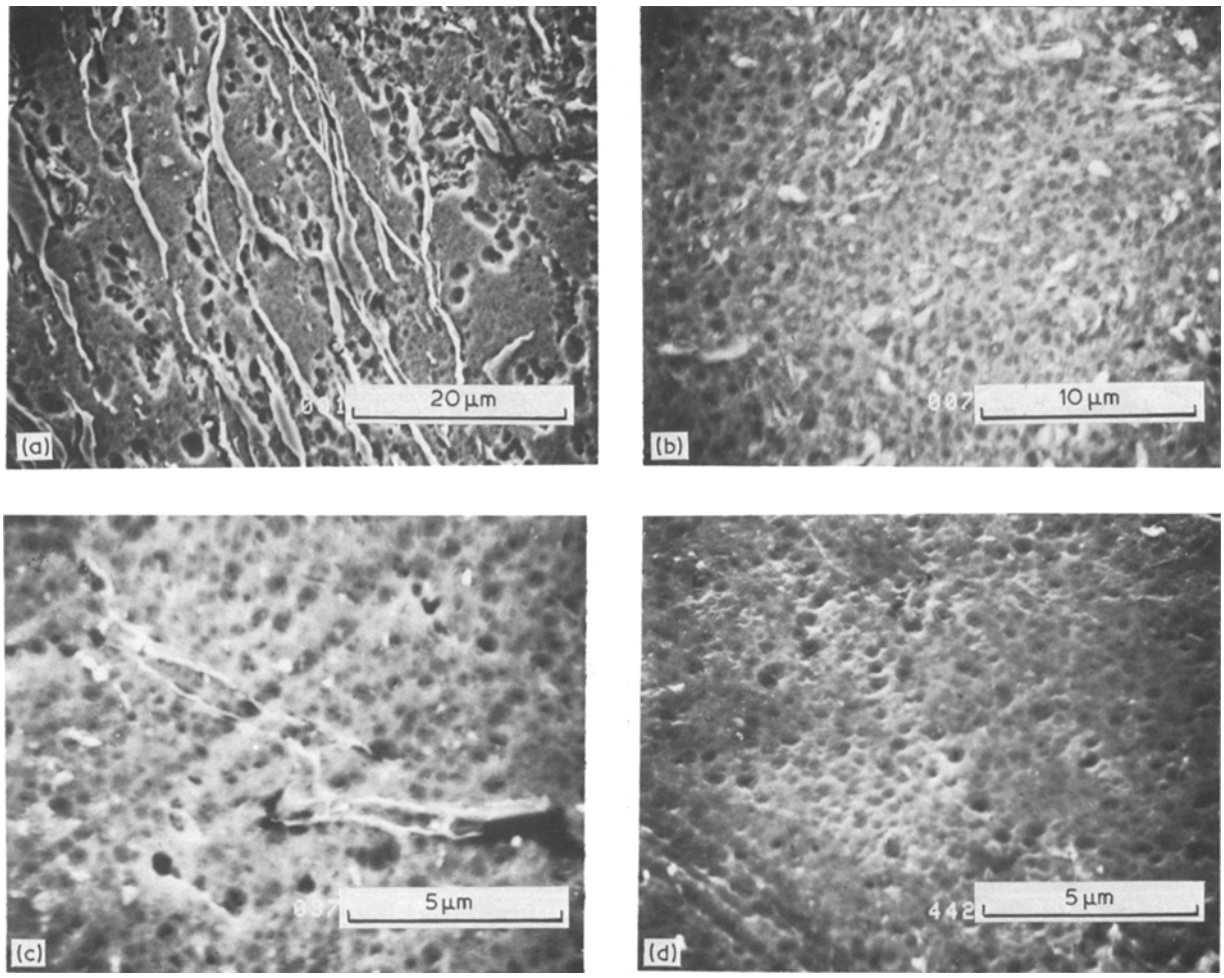

Figure 1 Scanning electron micrographs of $Ni_{40}Zr_{60}$ powder. Starting powder: nickel and $NiZr_2$. (a) 15 min, (b) 75 min, (c) 375 min, (d) 900 min. Pure nickel powder (white "strip") was embedded in the $NiZr_2$ intermetallic compound powder (pitted particles).

Products (Danvers, Massachusetts, USA). The $NiZr_2$, $Ni_{11}Zr_9$ and Ni_7Zr_2 intermetallic compounds were prepared by arc melting appropriate amounts of nickel and zirconium under zirconium-gettered argon, and were re-melted several times to ensure homogeneity. Powders were obtained by crushing the arc-melted buttons in a mortar and pestle. Table I shows the nominal composition and crystalline state of the starting powders. MA was carried out in a Spex Mixer/Mill using a hardened tool steel vial and 440C martensitic stainless steel balls. The vial was sealed with a vital O-ring in an argon-filled glove box. The ball to powder weight ratio was 10 : 1. Mechanically alloyed powders were characterized by X-ray diffraction measurements in a Debye–Scherrer powder camera and a GE XRD-5 diffractometer, both using Cu$K\alpha$ radiation and a nickel filter. Chemical analysis of the powders after mechanical alloying was performed by electron probe micro-analysis. The nickel and zirconium concentrations were within 1 at. % of the nominal composition. Oxygen analysis was made at Teledyne Wah-Chang Albany Company (Albany, Oregon, USA) using the inert-gas fusion technique. Thermal analyses were performed by means of a computerized differential scanning calorimeter (DSC, Dupont 9900 thermal analyser). The temperature scale was calibrated by using indium, zinc and K_2CrO_4 standards. Samples were heated in a purified argon atmosphere. A Hitachi-S530 scanning electron microscope was used to analyse MA powder morphology. Transmission electron microscopy was performed in a Hitachi-800 microscope operating at 200 kV. Specimens were electrochemically thinned using a solution of 35 ml perchloric acid, 165 ml butanol and 200 ml methanol at $-55°$ C.

3. Results and discussion

3.1. Scanning electron microscopy

3.1.1. MA of pure nickel with the intermetallic $NiZr_2$

The MA process consists of repeated mechanical mixing, cold welding, fracturing, and rewelding of ultrafine alloy powders [12]. The scanning electron micrographs in Fig. 1 reveal the effect of milling time on the development of particle structure during MA of pure nickel and the intermetallic $NiZr_2$. Fig. 1a shows the morphology of the $Ni_{40}Zr_{60}$ alloy after 15 min MA; it can be observed from the micrograph that the nickel powder was microforged into a "strip" shape due to repeated impacts between the milling balls and was cold welded with the $NiZr_2$ powders (present as pitted particles). The pitted surface is produced by the action of the etchant. It appears that the pure nickel strips are embedded in a granular $NiZr_2$ matrix, because $NiZr_2$ powders are the major component at this composition. As milling progresses, the nickel strip particles are further refined, as fracturing and cold welding of the powder particles continue. Figs 1b and c show typical

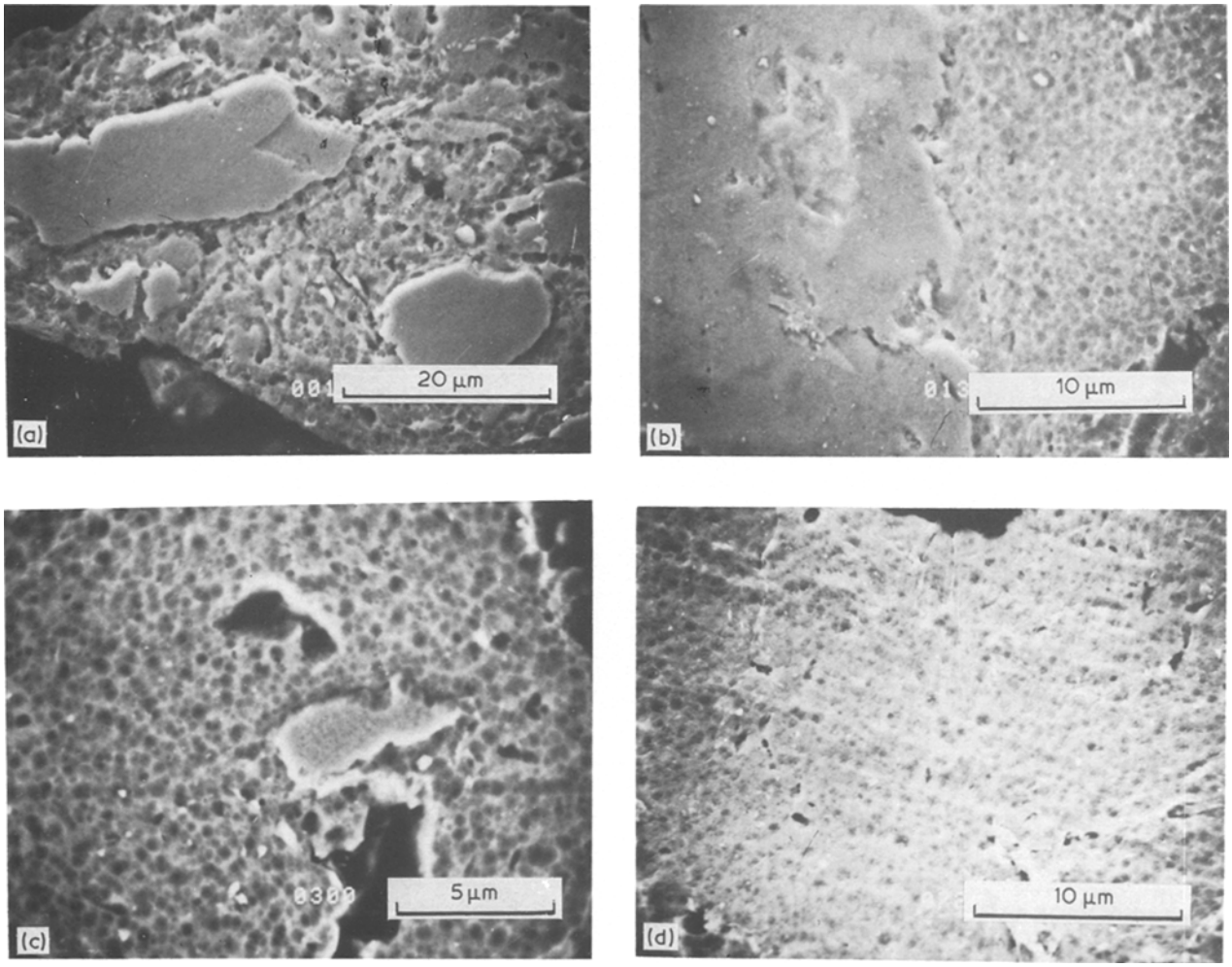

Figure 2 Scanning electron micrographs of $Ni_{40}Zr_{60}$ powder. Starting powder: $Ni_{11}Zr_9$ and $NiZr_2$. (a) 15 min, (b) 135 min, (c) 300 min, (d) 720 min. $Ni_{11}Zr_9$ intermetallic compound powder (smooth surface particles) was embedded in $NiZr_2$ intermetallic compound powder (pitted particles).

morphologies after 75 and 375 min milling, respectively. After 15 h milling, a single phase was observed as shown in Fig. 1d. At this stage the powders were found to have the amorphous structure.

3.1.2. MA of mixtures of intermetallic compounds

Fig. 2 shows a series of scanning electron micrographs which describe the structural development during formation of amorphous $Ni_{40}Zr_{60}$ powder by MA the intermetallics $NiZr_2$ and $Ni_{11}Zr_9$. The particle structure after 15 min milling is shown in Fig. 2a. It was found that $Ni_{11}Zr_9$ (minor component, smooth surface particle) is embedded in $NiZr_2$ particles (major component, pitted particle). With further milling, the $Ni_{11}Zr_9$ particles fractured into small fragments which were dispersed into the $NiZr_2$ particles. Figs 2b and c show the particle structures after 135 and 300 min, respectively. Finally, a single phase of amorphous $Ni_{40}Zr_{60}$ powder was observed after 12 h milling (Fig. 1d).

It is well known that a refined lamellar-type domain structure can be formed during the early stage of mechanically alloying two elemental ductile metal powders [12]. With further milling, the lamellar structure will be continually refined until the internal structure can no longer be revealed by optical microscopy or SEM [13]. However, examination of Figs 1 and 2 shows that the early stages of such a phenomenological mechanism does not appear in the present study. This difference is due to the replacement of part or all ductile elemental metal powder by brittle intermetallic

TABLE I The nominal composition and starting powder for MA of Ni_xZr_{1-x} alloys

Starting powder	x =											
	10–27	33	40	50	55	60	64	70	75	80	85	90
$Zr + NiZr_2$	×											
$NiZr_2$		×										
$Ni + NiZr_2$			×	×		×	×	×	×	×	×	×
$NiZr_2 + Ni_{11}Zr_9$			×	×								
$NiZr_2 + Ni_7Zr_2$					×				×			
$Ni_7Zr_2 + Ni$										×	×	×

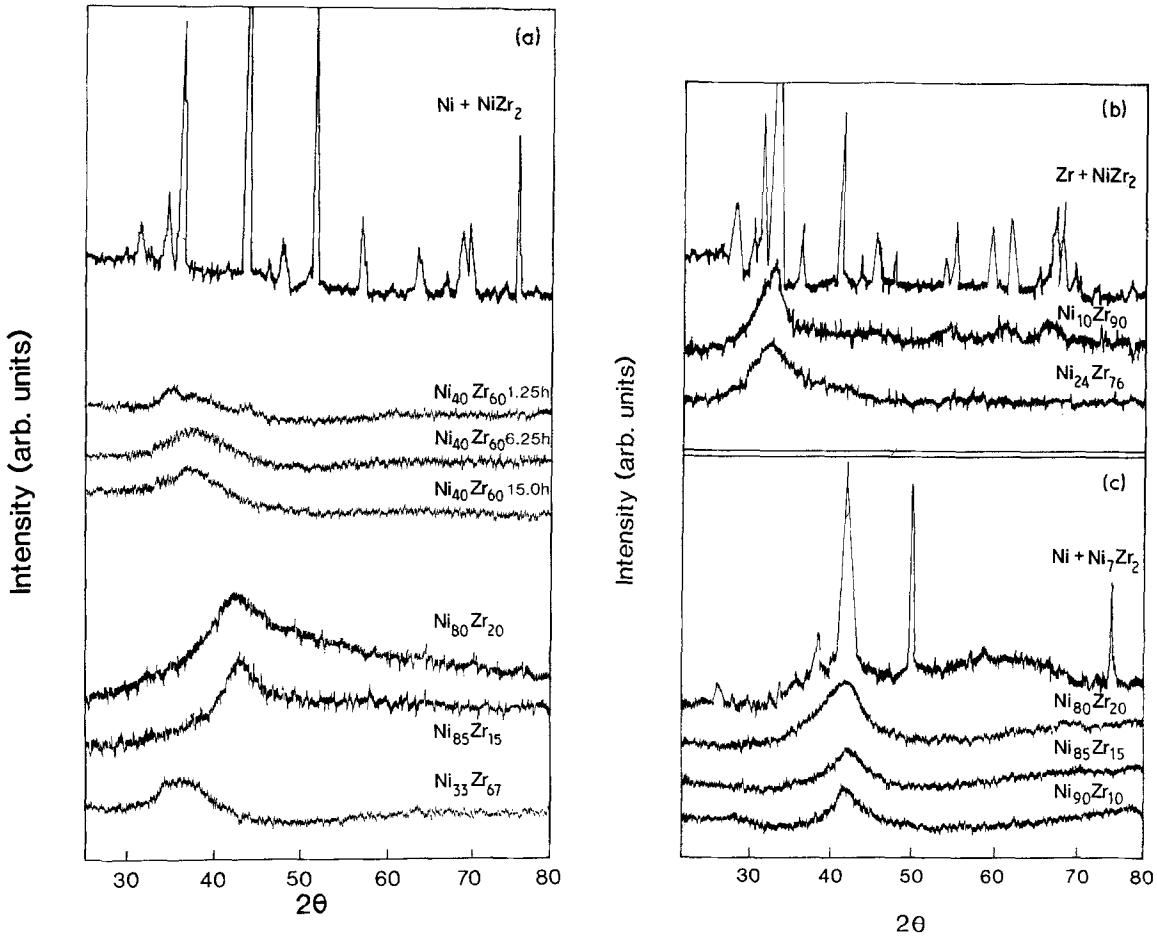

Figure 3 X-ray diffraction patterns of some representative Ni–Zr powders before and after mechanical alloying.

compound powder. It might be expected that MA of brittle components such as intermetallic compounds would result in continued fracture and particle pulverization. It is noted that Si–Ge solid solutions can be prepared by MA of brittle elements silicon and germanium, which indicated material can be transferred between brittle components [10]. Therefore, instead of the formation of a lamellar structure, the minor phase (nickel or $Ni_{11}Zr_9$) was dispersed into a major phase ($NiZr_2$).

3.2. X-ray diffraction

3.2.1. MA of mixtures of pure crystalline and intermetallic powders

MA of pure crystalline nickel and $NiZr_2$ intermetallic compound powder was carried out at compositions from $Ni_{40}Zr_{60}$ to $Ni_{90}Zr_{10}$. After a steady state condition (i.e. X-ray diffraction pattern stops changing with further milling) is reached during MA, the powders are amorphous for the composition range between $Ni_{40}Zr_{60}$ and $Ni_{80}Zr_{20}$. For $Ni_{85}Zr_{15}$, the powder is a mixture of the amorphous phase and the nickel-rich terminal solid solution fcc crystalline phase. Fig. 3a shows X-ray diffraction patterns of the starting powders and samples after MA of pure nickel and intermetallic $NiZr_2$. The starting powders show only $NiZr_2$ and nickel peaks. With increasing milling time, the peak intensities decrease and a broad amorphous peak develops between $2\theta = 32°$ and 44°. After 15 h milling, all the crystalline peaks have disappeared; only a broad peak is left, indicating amorphization is complete to the resolution of X-ray diffraction. The diffraction patterns of $Ni_{40}Zr_{60}$ and $Ni_{80}Zr_{20}$ shown in Fig. 3a represent the extreme range of amorphous Ni–Zr alloy that can be formed by MA of pure nickel and intermetallic $NiZr_2$ powders. In order to expand the range of amorphous Ni–Zr alloy powder formation, three kinds of starting powder were employed: intermetallic $NiZr_2$, pure zirconium with intermetallic $NiZr_2$, and pure nickel with intermetallic Ni_7Zr_2 powder. The X-ray diffraction patterns of Ni_xZr_{1-x} powders before and after MA of pure zirconium with $NiZr_2$ are shown in Fig. 3b. For $x = 0.24$ to 0.27, the powders are fully amorphous to the resolution of X-ray diffraction. For $x = 0.10$ to 0.22, a mixture of amorphous phase and hcp crystalline phase was detected. The formation of amorphous Ni–Zr alloy powder by MA of pure nickel with Ni_7Zr_2 also can be followed by examining the X-ray diffraction patterns shown in Fig. 3c. It is clear that amorphous $Ni_{80}Zr_{20}$ and $Ni_{85}Zr_{15}$ alloy powders were formed. It is also shown that a mixture of amorphous and crystalline phases were detected for $Ni_{90}Zr_{10}$ powder. Examination of Fig. 3a shows that $Ni_{33}Zr_{67}$ amorphous powder can be formed by milling the intermetallic $NiZr_2$ powder.

3.2.2. MA of mixtures of intermetallic compounds

Four compositions ($Ni_{40}Zr_{60}$, $Ni_{50}Zr_{50}$, $Ni_{55}Zr_{45}$ and $Ni_{75}Zr_{25}$) have been chosen for the investigation of the formability of Ni–Zr amorphous powder by MA of

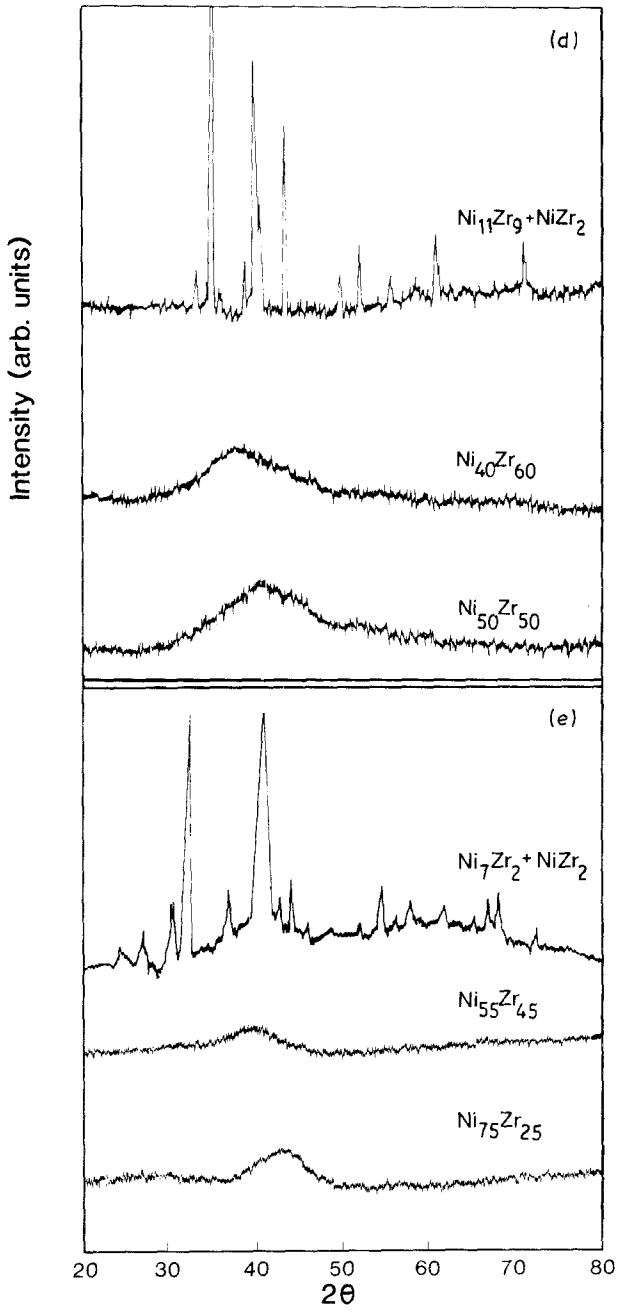

Figure 3 Continued.

mixtures of intermetallic compounds. Figs 3d and e show X-ray diffraction patterns of the mixtures before and after MA. The diffraction peaks of the top curve in each figure correspond to the mixture of $Ni_{11}Zr_9$ and $NiZr_2$ (Fig. 3d) and $NiZr_2$ and Ni_7Zr_2 (Fig. 3e) intermetallic compound powders. The other four curves are the diffracted intensity of the $Ni_{40}Zr_{60}$, $Ni_{50}Zr_{50}$, $Ni_{55}Zr_{45}$ and $Ni_{75}Zr_{25}$ powders after 8, 18, 26 and 36 h MA, respectively. The structure of these alloys is considered to be essentially amorphous to the resolution of our X-ray diffraction measurements.

Therefore, from X-ray diffraction, it is found that by MA of intermetallics, mixtures of pure crystalline and intermetallic compound powders, and mixtures of intermetallic compound powders, an amorphous Ni_xZr_{1-x} powder was formed for $x = 0.24$ to 0.85. For $x = 0.10$ to 0.22 and 0.90, the Ni_xZr_{1-x} powder is a mixture of an amorphous phase and crystalline phases.

3.3. Transmission electron microscopy

TEM studies were performed to characterize the microstructure of the amorphous Ni–Zr alloy powders. The amorphous $Ni_{50}Zr_{50}$ powders starting from different powder mixtures, i.e. Ni + $NiZr_2$ or $Ni_{11}Zr_9$ + $NiZr_2$, were chosen for investigation. Bright-field transmission electron micrographs of amorphous $Ni_{50}Zr_{50}$ powders are shown in Figs 4 and 5. Both bright-field micrographs show a "salt and pepper" contrast typical of amorphous material and the diffraction pattern exhibits only the broad diffuse ring typical of an amorphous structure. The bright-field micrographs also show the "black band" ribbon shape which is likely to be a surface artefact of the electropolishing of this reactive alloy. A very few small bright areas (less than 0.5% of the sample volume) can be observed in the dark-field micrograph (Fig. 4b). These areas might be the presence of tiny crystallites ($\sim$ 10 nm diameter). However, the corresponding electron diffraction pattern indicates most of the powder is amorphous.

3.4. Thermal analysis

The amorphous powders were heated at different rates in the differential scanning calorimeter (DSC) in order to study their crystallization behaviour. Fig. 6 shows some examples of DSC measurements for the amorphous Ni–Zr alloys, with a scanning rate of 10 K min^{-1}. The sharp exothermic peak at high temperatures indicates crystallization, which was confirmed by subsequent X-ray diffraction measurements. The crystallization temperatures were defined from the peak position of the first peak in the DSC scans. Fig. 7a shows the crystallization temperature as a function of composition. These values correspond to a scan rate of 10 K min^{-1}. The points in parentheses are for the partially amorphous alloys at the extremes of the glass-forming range. A maximum in crystallization temperature was observed at a zirconium content near 36%. Previous results of melt-spun amorphous Ni–Zr samples [14] showed a different crystallization temperature–composition dependence: (1) two maxima were observed at zirconium concentrations around 36% and 55%; (2) at compositions between 36 to 55% Zr and 67 to 80% Zr, the crystallization temperatures are lower than samples prepared by MA.

Fig. 7b shows the enthalpies of crystallization (ΔH_c) which were determined from the appropriate areas under the DSC traces. Altounian *et al.* [14] have reported that variation of ΔH_c with concentration provides a guide to the crystalline phase diagram in Ni–Zr amorphous alloys; a maximum ΔH_c corresponds to an intermetallic compound, and a minimum ΔH_c relates to a eutectic. However, this trend does not clearly appear in our work. A similar study on the thermal properties of MA Ni–Nb amorphous powders also did not show such a trend [15].

The activation energies for crystallization (E_c) were determined from the shift in crystallization temperature with heating rate, using Kissinger's method [16]. The results are shown in Fig. 7c. A different E_c–composition dependence was found between MA and melt-spun samples [14]. The values of ΔH_c and E_c

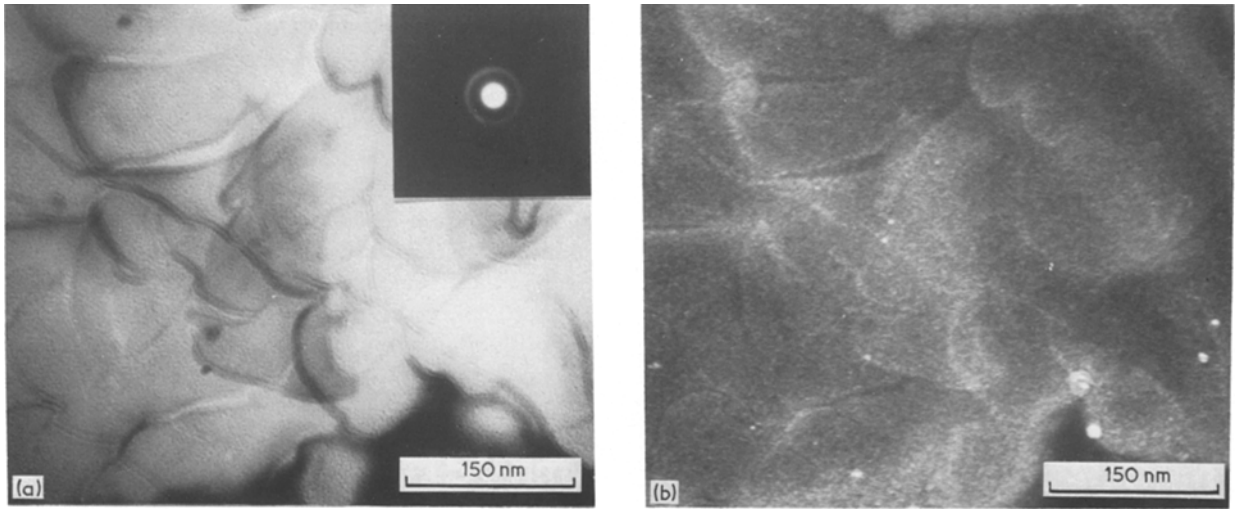

Figure 4 Transmission electron micrographs of amorphous $Ni_{50}Zr_{50}$ alloy powder after MA of the mixture of $Ni_{11}Zr_9$ and $NiZr_2$ intermetallic compound powder. (a) Bright field, (b) dark field.

for MA samples measured in the present study are lower than those for melt-spun samples [14]. A similar tendency also has been observed for MA Ni–Nb amorphous alloys when compared with melt-spun samples [15]. The possible reasons for the difference in thermal stability between MA and melt-spun amorphous alloys will be discussed below.

4. Discussion

4.1. Driving force for amorphization

4.1.1. MA of mixtures of intermetallic compounds

Many binary transition metal alloys have been amorphized by MA of mixtures of pure crystalline powders [4–6]. The driving force for this transformation is the large negative heat of mixing in the systems studied to date which makes the free energy state of the amorphous alloys lower than that of the crystalline mixture. This cannot be the case when the starting powders are the equilibrium intermetallic compounds.

The following thermodynamic arguments can be made to rationalize amorphization by MA in these cases. A free energy diagram of the Ni–Zr system has been calculated for a temperature of 338 K based on the method which is described by Schwarz *et al.* [4]. Examination of Fig. 8 shows that the equilibrium free energy of the mixtures of $Ni_{11}Zr_9$ + $NiZr_2$ powders for an average composition of $Ni_{40}Zr_{60}$ is located at G_0. Brimhall *et al.* [17] have suggested that for intermetallic compounds with narrow ranges of homogeneity, i.e. "line" compounds, only a slight deviation

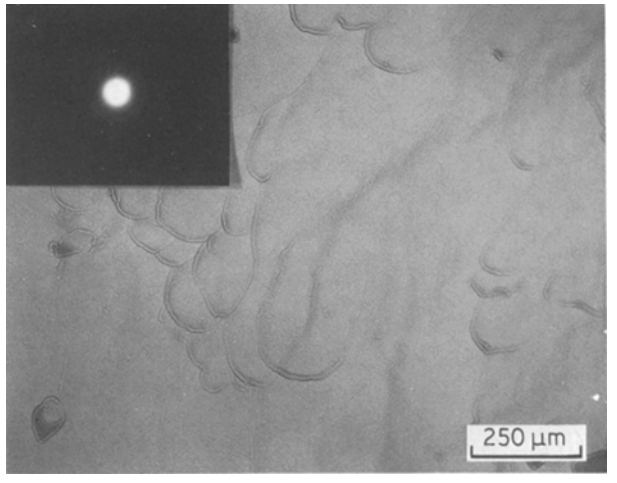

Figure 5 Transmission electron micrograph of amorphous $Ni_{50}Zr_{50}$ alloy powder after MA of the mixture of pure nickel and $NiZr_2$ intermetallic compound powder.

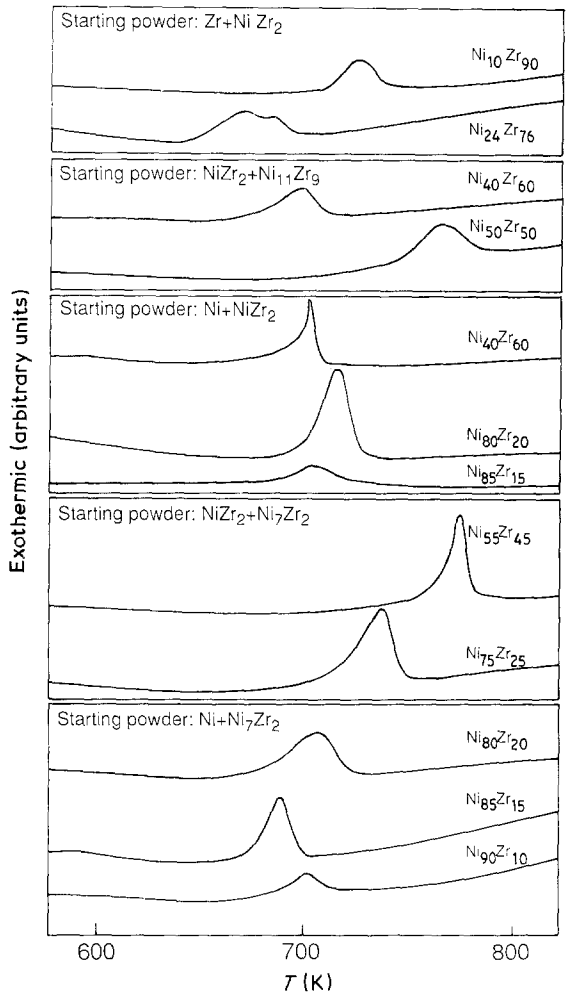

Figure 6 DSC scans at 10 K min^{-1} for a series of Ni–Zr amorphous powders.

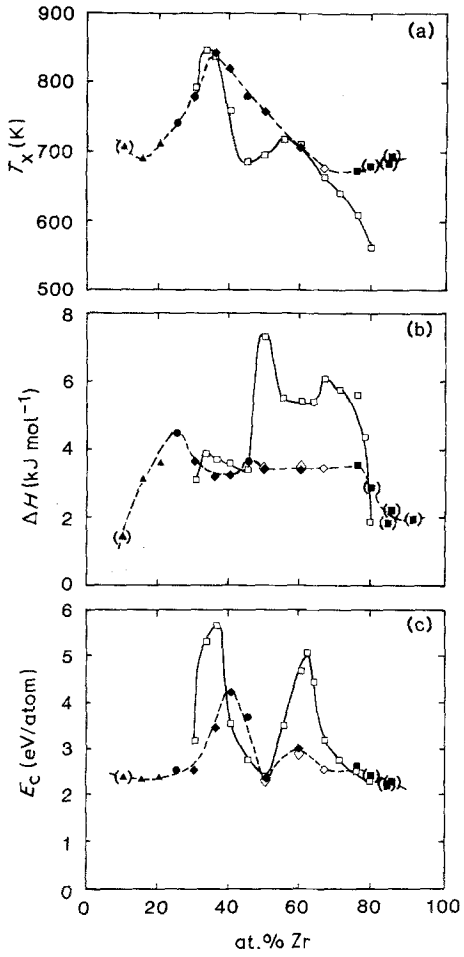

Figure 7 (a) The crystallization temperature, (b) enthalpy of crystallization and (c) activation energy for crystallization, of amorphous Ni–Zr powders. (▲) Ni_7Zr_2 + Ni, (◆) $NiZr_2$ + Ni, (■) Zr + $NiZr_2$, (◇) $NiZr_2$, (●) Ni_7Zr_2 + $NiZr_2$, (◇) $NiZr_2$ + $Ni_{11}Zr_9$, (□) Altounian *et al.* [14].

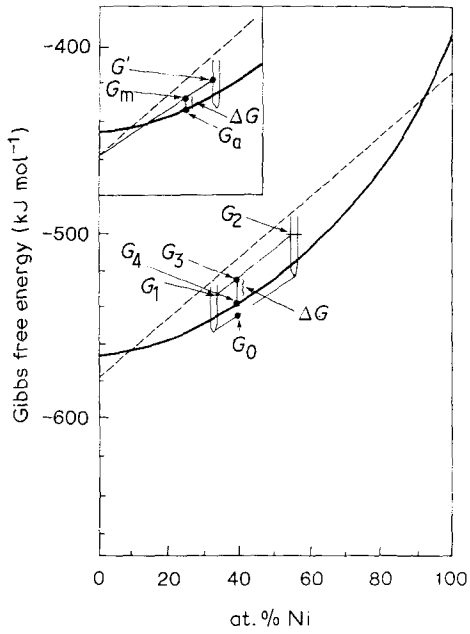

Figure 8 Free energy diagram for the binary Ni–Zr system. The heavy solid line represents the amorphous state, the thin lines represent the intermetallic compounds and the dashed line represents the mixture of elemental crystalline powders.

beyond the stoichiometric concentration results in a large rise in the free energy. As non-equilibrium material transfer occurs during MA of $Ni_{11}Zr_9$ and $NiZr_2$ the compositions of the two compounds may be shifted toward the average $Ni_{40}Zr_{60}$ alloy. The compounds will now have compositions off-stoichiometry and the free energies will rise, respectively, to values, for example, represented by $G_1(NiZr_2)$ and $G_2(Ni_{11}Zr_9)$. The free energy of the mixture of off-stoichiometric intermetallics will then be G_3, which is larger than for that of the corresponding amorphous alloy at G_4. Thus $\Delta G = G_3 - G_4$ could act as the driving force for amorphization. An alternative explanation is based on a critical defect concentration. It is noted that $Ni_{33}Zr_{67}$ amorphous powder can be formed by milling the intermetallic compound $NiZr_2$. Schwarz and Koch [8] have prepared amorphous $Ni_{45}Nb_{55}$ and $Ni_{32}Ti_{68}$ powders by ball milling the respective crystalline intermetallics, Ni_6Nb_7 and $NiTi_2$. These results indicate that the free energy of the equilibrium intermetallic compounds might be raised by the accumulation of crystal defects created by the mechanical attrition. When a critical defect concentration is attained such that the free energy of the defect-containing intermetallic is equal to or greater than that of the amorphous alloy, a transition to the amorphous phase may occur. MA of mixtures of intermetallics could proceed by, first, amorphization of each compound by the above mechanism. Alloying of the two amorphous phases would then proceed with continued MA. Thus, we have a classic problem in diffusional phase transitions: which occurs first – the structure change or the compositional change? Research in progress to identify better the dominant mechanism of amorphization in this case is emphasizing structural studies by X-ray diffraction and transmission electron microscopy of the evolution of the amorphous phase.

4.1.2. MA of mixtures of elements and intermetallic compounds

The driving force for producing amorphous alloys by MA of mixtures of elemental zirconium and $NiZr_2$ intermetallic compound powders is similar to the case discussed in Section 4.1.1. During initial milling, the free energy of the intermetallic was raised steeply to G' as material transfer moves its composition off-stoichiometry, thus making the free energy of the mixture (G_m) higher than the free energy of the corresponding amorphous alloy (G_a). Therefore $\Delta G = G_m - G_a$ could act as the driving force for amorphization. The corresponding free energy change is shown on the left corner of Fig. 8.

4.2. Formation range of the amorphous state

Amorphous Ni–Zr alloy powder can be formed in a concentration range from 24 to 85 at. % Ni by MA of powder mixtures with different crystalline states. This range is larger than amorphous alloys produced by either MA of elemental crystalline powders (20 to 70 at. % Ni [18]) or by the melt-spinning technique (20 to 70 at. % Ni and 90 at. % Ni, [14, 19]; 22 to 71 at. % Ni and 91 at. % Ni [20]). The formation of amorphous Ni–Zr alloys at compositions between 70 and 90 at. % Ni has never been attained by the melt-spinning technique. The absence of a eutectic and the

TABLE II Crystallization products of amorphous Ni_xZr_{1-x} powders

x =	Starting powder	Intermediate stage	Final products
24	$Zr + NiZr_2$	hcp	hcp + γ
33	$NiZr_2$	–	$NiZr_2$
40	$Ni + NiZr_2$	NiZr	$NiZr + NiZr_2$
	$Ni_{11}Zr_9 + NiZr_2$	NiZr	$NiZr + NiZr_2$
50	$Ni + NiZr_2$	–	NiZr
	$Ni_{11}Zr_9 + NiZr_2$	–	NiZr
80	$Ni + Ni_7Zr_2$	–	$Ni_7Zr_2 + Ni_5Zr$
85	$Ni + Ni_7Zr_2$	–	Ni_5Zr + fcc
90	$Ni + Ni_7Zr_2$	–	Ni_5Zr + fcc

hcp = zirconium solid solution. fcc = Ni solid solution. $\gamma = NiZr_3O_{0.115}$.

presence of line compounds in this composition range are presumably responsible for the inability to form glasses by rapid solidification. In contrast to this, MA of either mixtures of line compounds ($NiZr_2 + Ni_7Zr_2 \rightarrow$ a-$Ni_{75}Zr_{25}$) or mixtures of pure nickel and a line compound ($Ni + Ni_7Zr_2 \rightarrow$ a-$Ni_{85}Zr_{15}$) can lead to formation of the amorphous state. This demonstrates that the two processes are significantly different. Thus, some restrictions of the melt-spinning technique can be overcome by the MA process.

4.3. Crystallization behaviour

4.3.1. Products of crystallization

X-ray diffraction studies were performed on all samples after heating in the DSC to analyse the structure of the intermediate and final phases formed after crystallization. The results are summarized in Table II. At compositions from $Ni_{10}Zr_{90}$ to $Ni_{27}Zr_{73}$, crystallization involves two distinct stages, as determined from two peaks in DSC traces. X-ray diffraction patterns were made on samples quickly cooled from either the temperature of the first or second peak of the DSC traces. The first exotherm corresponds to the precipitation of the hcp zirconium-rich terminal solid solution, an equilibrium phase. The second exotherm was associated with the formation of the ternary γ-phase. This phase is known to exist in the system Ni–Zr–O [21]. The crystal structure of the γ-phase has not been identified. The γ-phase has the $NiZr_3$ metal component stoichiometry with oxygen concentrations ranging from about 6 to 19 at. %. The oxygen contents of as-MA $Ni_{22}Zr_{78}$ and $Ni_{24}Zr_{76}$ powders are 3.9 and 2.3 at. %, respectively. After annealing in the DSC, the oxygen levels increased to 12.4 and 15.7 at. %, respectively. This implies considerable oxygen contamination during heating in the DSC. Assuming all the oxygen is involved with the formation of the γ-phase, an oxide of $NiZr_3O_x$ with $x = 0.577$ to 0.800 will be formed, where oxygen content = 12.6 to 17.0 at. %. In order to avoid oxidation, $Ni_{24}Zr_{76}$ amorphous powder was annealed at 750 K for 10 min inside a vacuum furnace at a pressure of 10^{-6} torr. The oxygen content after annealing was 2.7 at. %. X-ray diffraction was carried out after the anneal, and the products of crystallization were identified to be the hcp terminal solid solution and γ-oxide. Again, assuming all oxygen is involved on the formation of the γ-phase, an oxide of $NiZr_3O_{0.115}$ will be formed, where oxygen content = 2.9 at. %. This is a metastable phase because the equilibrium γ-oxide phase has a range of oxygen concentrations from about 6 to 19 at. %.

4.3.2. Thermal properties

Examination of Fig. 6 indicates that most of the enthalpies and activation energies of crystallization of the amorphous alloys of the present work are lower than those alloys previously prepared by melt spinning [14]. It also shows that at compositions between 36 to 55% Zr and 67 to 80% Zr, the crystallization temperature of the amorphous alloys of the present work are higher than melt-spun samples [14]. MA is a ball milling process involving fine powders (~ 1 to 5 μm diameter) and a large surface to volume ratio. The contamination by oxygen of MA samples might be larger than melt-spun samples and may influence the crystallization behaviour of MA amorphous powders. The effect of oxygen content on the temperature and activation energy for crystallization of MA

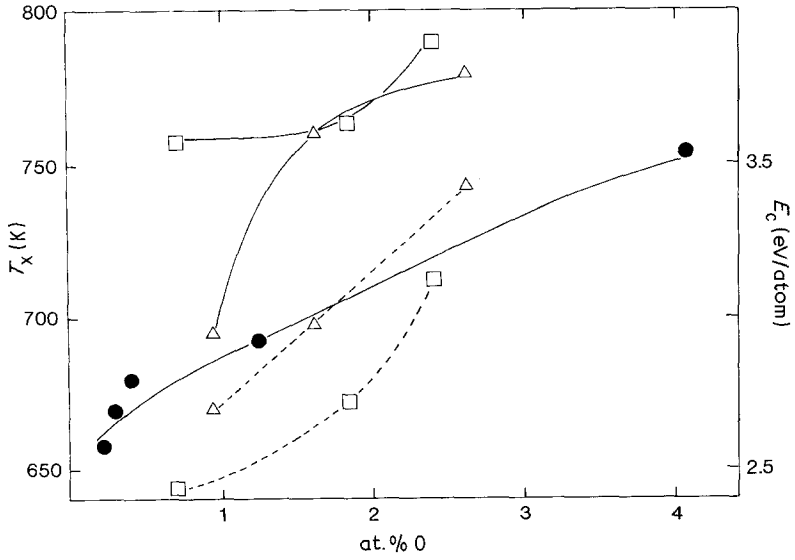

Figure 9 Temperature (T_x ——) and activation energy (E_c – – –) for crystallization of (△) $Ni_{40}Zr_{60}$, (●) $Ni_{33}Zr_{67}$, and (□) $Ni_{50}Zr_{50}$ amorphous powders as a function of oxygen content.

$Ni_{40}Zr_{60}$ and $Ni_{50}Zr_{50}$ amorphous powders is shown in Fig. 9. When oxygen content increases, the temperature and activation energy for crystallization increases. Altounian *et al.* [22] found the same behaviour with the melt-spun $NiZr_2$ amorphous alloy. MA is a solid state amorphizing reaction, therefore some partial crystallinity after MA may be expected and has been observed. The small bright areas appearing on the dark-field transmission electron micrograph of $Ni_{40}Zr_{60}$ (Fig. 4a) are presumably tiny crystallites. These areas might act as nucleation centres during crystallization, thus lowering the thermal stability of MA amorphous powders. Altounian *et al.* [14] have reported that the presence of a small volume fraction of crystallites has caused the drop of T_x in the melt-spun $Ni_{55}Zr_{45}$ amorphous alloy. The crystallization behaviour of amorphous materials is complicated, with many variables influencing the mode and kinetics of crystallization [23]. It may not be sufficient to explain the differences in thermal properties between MA Ni–Zr amorphous powders and melt-spun Ni–Zr samples only by the combined effects of residual crystallinity and different oxygen levels. A more detailed study of the crystallization behaviour of MA amorphous powder is needed.

5. Conclusions

Amorphous Ni–Zr alloys have been synthesized by mechanical alloying of powder mixtures with different crystalline states: (1) mixtures of pure crystalline powders with intermetallic powders, (2) mixtures of intermetallic powders. The results obtained are summarized as follows.

1. Amorphous Ni_xZr_{1-x} alloy powder has been synthesized in the range $0.24 \leqslant x \leqslant 0.85$ by mechanical alloying. This range is larger than amorphous alloys produced by the melt-spinning technique or by mechanical alloying of elemental crystalline powders. A mixture of amorphous and crystalline phases formed in the composition range of $0.10 \leqslant x \leqslant 0.22$ and $x = 0.90$.

2. The driving force for the amorphization of mixtures of intermetallics is believed to be either the steep rise in the free energy of the line compounds as material transfer moves their compositions off-stoichiometry, or the creation of a critical defect concentration in the intermetallic compounds.

3. The enthalpy and activation energy for crystallization of the MA Ni–Zr amorphous powders are lower than for melt-spun samples. The temperature for crystallization of the MA Ni–Zr amorphous powders is higher than the melt-spun samples in the composition range $Ni_{20}Zr_{80}$ to $Ni_{33}Zr_{67}$ and $Ni_{40}Zr_{60}$ to $Ni_{60}Zr_{40}$. Oxygen increases the crystallization temperature and activation energy for crystallization of the $Ni_{40}Zr_{60}$ and $Ni_{50}Zr_{50}$ amorphous powders.

4. After crystallization of $Ni_{24}Zr_{76}$ amorphous powder, a non-equilibrium γ-phase-$NiZr_3O_x$ ($x = 0.115$) was detected.

Acknowledgements

The authors wish to thank S. A. Myers for TEM assistance. This research was sponsored by the US National Science Foundation under NSF Grant no. DMR-8318561.

References

1. F. E. LUBORSKY (ed.), "Amorphous Metallic Alloys" (Butterworths, London, 1983).
2. R. B. SCHWARZ and W. L. JOHNSON, *Phys. Rev. Lett.* **51** (1983) 415.
3. C. C. KOCH, O. B. CAVIN, C. G. McKAMEY and J. O. SCARBROUGH, *Appl. Phys. Lett.* **43** (1983) 1017.
4. R. B. SCHWARZ, R. R. PETRICH and C. K. SAW, *J. Non-Crystalline Solids* **76** (1985) 281.
5. C. POLITIS, Proceedings of the 6th International Conference on Liquid and Amorphous Metals, August 1986, Garmisch-Partenkirchen, West Germany.
6. E. HELLSTERN and L. SCHULTZ, *Appl. Phys. Lett.* **48** (1986) 124.
7. R. B. SCHWARZ, *Mater. Res. Soc. Bull.* **May/June** (1986) 55.
8. R. B. SCHWARZ and C. C. KOCH, *Appl. Phys. Lett.* **49** (1986) 146.
9. C. C. KOCH and M. S. KIM, *J. Physique* **46** (1985) C8-573.
10. R. M. DAVIS and C. C. KOCH, *Scripta Metall.* **21** (1987) 305.
11. P. Y. LEE and C. C. KOCH, *Appl. Phys. Lett.* **50** (1987) 1578.
12. J. S. BENJAMIN, *Sci. Amer.* **234** (1976) 40.
13. B. P. DOLGIN, M. A. VANEK, T. McGORY and D. J. HAM, *J. Non-Crystalline Solids* **87** (1986) 281.
14. Z. ALTOUNIAN, TU GUO-HA and J. O. STROM-OLSEN, *J. Appl. Phys.* **54** (1983) 3111.
15. P. Y. LEE and C. C. KOCH, *J. Non-Crystalline Solids* **94** (1987) 88–100.
16. H. E. KISSINGER, *Anal. Chem.* **29** (1957) 1702.
17. J. L. BRIMHALL, H. E. KISSINGER and L. A. CHARLOT, *Radiat. Eff.* **77** (1983) 237.
18. F. PETZOLDT, B. SCHOLZ and H. D. KUNZE, in Proceedings of the 6th International Conference on Rapidly Quenched Metals, Montreal 1987.
19. Z. ALTOUNIAN, E. BATALLA and J. O. STROM-OLSEN, *J. Appl. Phys.* **59** (1986) 2364.
20. K. H. J. BUSCHOW, *J. Phys. F Met. Phys.* **14** (1984) 593.
21. M. V. NEVITT and J. W. DOWNEY, *Trans. Met. Soc. AIME* **221** (1961) 1017.
22. Z. ALTOUNIAN, E. BATALLA and J. O. STROM-OLSEN, *J. Appl. Phys.* **61** (1987) 149.
23. H. J. GUNTHERODT and H. BECK (eds), "Topics in Applied Physics" (Springer, Berlin, 1981) p. 225.

Received 20 August
and accepted 1 December 1987